Colloids and Surfaces B: Biointerfaces 71 (2009) 169–176

Contents lists available at ScienceDirect

Colloids and Surfaces B: Biointerfaces

journal homepage: www.elsevier.com/locate/colsurfb

In-situ monitoring of *Cryptosporidium parvum* oocyst surface adhesion using ATR-FTIR spectroscopy

Xiaodong Gao, Jon Chorover*

Department of Soil, Water and Environmental Science, University of Arizona, Tucson, 85721 AZ, United States

ARTICLE INFO

Article history:
Received 20 November 2008
Received in revised form 31 January 2009
Accepted 2 February 2009
Available online 13 February 2009

Keywords:
Oocysts
ATR-FTIR
Adhesion
Solution chemistry
Surface modification

ABSTRACT

Surface chemistry and molecular interaction mechanisms of *Cryptosporidium parvum* oocysts with a ZnSe internal reflection element (IRE) surface were investigated as a function of pH and ionic strength in NaCl and $CaCl_2$ background electrolyte using in-situ ATR-FTIR spectroscopy. Since the surface properties of oocysts play an important role in adhesion behavior, the effects of surface modifications that are commonly employed to inactivate the pathogen for laboratory studies, including viable (control), formalin-, and heat-inactivation, were also examined.

The ATR-FTIR spectra of oocyst surfaces exhibit amide, carboxylate, phosphate, and polysaccharide functional groups. Results indicate that changes in solution chemistry strongly impact oocyst adhesion behavior in aqueous systems. Increasing ionic strength from 1 to 100 mM or decreasing pH from 9.0 to 3.0 resulted in an increase in oocyst adhesion to the IRE surface as measured by IR absorbance. For equivalent ionic strength, the adhesion rate was found to be independent of $CaCl_2$ versus NaCl electrolyte solution, but was increased following formalin and heat treatments. This latter effect correlated with molecular changes reflected in spectral data. The ratio of amide I:amide II band intensities increased, and sugar ring vibrations at 1023 cm^{-1} became sharper and more intense following formalin treatment. Similar changes in the polysaccharide region were observed following heat treatment, and protein secondary structure was also altered from mainly parallel β-sheet to anti-parallel β-sheet conformation.

1. Introduction

Cryptosporidium parvum is an enteric parasite that causes the diarrheal disease Cryptosporidiosis in humans and other mammals. Oocysts are the encysted, environmental form of this obligate pathogen, which can be transported in surface water, groundwater, and soils. Once ingested, the oocysts excyst in the small intestine and result in an infection of intestinal epithelial tissue. Ranging in diameter from 3 to 6 μm [1], oocysts are spherical to slight ovoid in shape with a thick cell wall. Due to their widespread occurrence in drinking water supplies and their strong resistance to various environmental stresses, including freezing, desiccation, and chlorination, *C. parvum* oocysts are considered one of the most challenging microbial parasites in drinking water systems [2,3]. A number of large outbreaks of *C. parvum* have been reported in recent years in the U.S., as well as in other countries. The most notable outbreak in Milwaukee, WI in 1993 was responsible for 400,000 illnesses, 4000 hospitalizations, and 104 deaths [4].

Due to the potential health threat, the fate and transport of oocysts in the environment have been studied extensively in the past decade. Most of these studies examined oocyst transport behavior under various solution chemistry conditions (e.g. pH, ionic strength) using classical column experiments at the bench scale in packed granular porous media, such as pure quartz sand, Fe oxide-coated sand, and natural soils [5–9]. The results from these studies demonstrate that oocyst transport behavior and removal rates depend on adsorbent properties (e.g., particle size and composition) and solution chemistry (e.g., pH and ionic strength). The influence of cation composition and natural organic matter (NOM) has been studied as well [10–12]. However, the specific mechanisms of surface interaction and, in particular, the role of molecular-scale surface chemistry of the oocysts themselves, are still poorly resolved.

The surface chemistry of microorganisms – including hydrophobicity, surface charge, and surface molecular structure – mediates cell adhesion to solid surfaces and, therefore, controls transport and removal processes in aqueous environments [3]. The influence of surface charge and van der Waals interactions, in particular, are incorporated into Derjaguin–Landau–Verwey–Overbeek (DLVO) models of interfacial forces that govern adhesion [13]. *C. parvum* oocysts exhibit an isoelectric point (IEP) of ~2.0–3.3 depending on solution ionic strength [10,14–17], indicating negative surface

* Corresponding author. Tel.: +1 520 626 5635; fax: +1 520 621 1647.
E-mail address: chorover@cals.arizona.edu (J. Chorover).

0927-7765/$ – see front matter © 2009 Elsevier B.V. All rights reserved.
doi:10.1016/j.colsurfb.2009.02.003

charge for conditions encountered in most natural waters. In addition, oocysts exhibit hydrophilic properties [11,12,15,18], because polar functional groups populate the external surface. However, the influence of treatment processes that are used to inactivate oocysts for safe use in laboratory experiments may alter some of the key properties that affect adhesion. For example, reaction of oocysts with formalin, which is among the most commonly used methods of oocyst inactivation, was reported to substantially increase hydrophobicity, but the underlying reason is unclear [18].

Kuznar and Elimelech [18,19] modified oocyst surfaces with formalin, heat, and proteinase K treatments to study treatment effects on kinetics of deposition on silica using a radial stagnation point flow system (RSPF). They reported that the surface treatments did not significantly affect the pH-dependence of oocyst electrophoretic mobility (relative to viable cells), which suggests no substantial change in the electrostatic repulsive force between oocysts and silica particles. However, they obtained much higher attachment efficiencies after treatment suggesting a non-DLVO repulsive force is diminished. Several recent atomic force microscope (AFM) studies [10,20–22] also suggest that the surface interaction of oocysts cannot be fit to the traditional DLVO model force at short-range <30 nm. The additional repulsion has been attributed to a short-range "electrosteric force" that is thought to result from a layer of surface proteins extending into solution as a brush-like structure. Byrd and Walz [21,22] reported that repulsion between oocysts and silica particles is essentially dominated by this short-range steric force. They proposed that the oocyst surface is composed of a thin layer of charged proteins bonded covalently to a thick layer of uncharged carbohydrates (e.g. polysaccharides). The positive influence of dissolved Ca^{2+} on adhesion was attributed to the ability of this bivalent cation to effectively compress the biopolymer layer [10].

Although these prior AFM and RSPF studies suggest the importance of surface biomolecules to oocyst adhesion interactions, details on their molecular structure and functional group chemistry remain limited. It is known that the oocyst cell wall is *ca*. 40–50 nm thick, and is dominated by acidic glycoproteins comprising cysteine, proline, and histidine [23,24]. These glycoproteins are thought to contribute to the hairy layer extending from the surface that prevents direct adhesion to soil particles [10,20]. By fitting pK_a values to surface titrations, Karaman et al. [16] proposed that carboxylate and phosphate groups are likely prevalent at the oocyst surface, but no direct evidence was provided.

Attenuated total reflectance-Fourier transform infrared (ATR-FTIR) spectroscopy is a surface-sensitive technique that provides molecular-scale information on oocyst interfaces immersed in aqueous solution. In addition, ATR-FTIR is sensitive to protein secondary structure, so biomolecular alterations resulting from oocyst pretreatment or solution chemistry effects may be detected in-situ. ATR-FTIR spectroscopy has been employed to elucidate the surface chemistry of bacteria and molecular processes governing their interaction with mineral substrates [25–31]. We are aware of only one prior ATR-FTIR study of *C. parvum* oocysts [32]. However, the quality of the spectra was insufficient to clearly elucidate functional group chemistry, and the work did not include a systematic study of solution chemistry or oocyst treatment effects.

The first objective of this study was to obtain surface functional group composition for oocysts in aqueous solutions, and to measure the adhesion of oocysts to the ZnSe internal reflection element (IRE) surface using in-situ ATR-FTIR spectroscopy. Specifically, we measured the variation of band frequencies and intensities as a function of pH, ionic strength, ionic composition, and time. Oocysts were equilibrated with a range of aqueous solutions, deposited on a ZnSe IRE, and then spectra were collected as a function of pH from 3 to 9 and ionic strength from 1.0 to 100 mM in both NaCl and $CaCl_2$ background electrolytes over a period of 24 h. Infrared absorbance was used as a measure of adhesion.

Our second objective was to assess the effects of common oocyst inactivation treatments on ATR-FTIR detectable changes in surface chemistry. Formalin and heat treatment are the most commonly used and effective methods to inactivate viable oocysts for laboratory transport studies. Nonetheless, it has been shown that resulting surface modifications can significantly alter the rate and extent of oocyst deposition [18,19,21,22]. Hence, the effect of the different surface modifications, including viable (control), formalin-, and heat-inactivation, was also examined in this study.

2. Materials and methods

2.1. C. parvum oocyst preparation

All *C. parvum* oocysts used in this study were provided by the Sterling Parasitology Laboratory (SPL) at the University of Arizona. The oocysts were shed from a calf infected with the Iowa Isolate of *C. parvum* at the National Animal Disease Center in Ames, IA. Oocysts were purified at SPL by discontinuous sucrose and cesium chloride (CsCl) centrifugation gradients. Formalin inactivation was conducted at SPL by contacting the oocysts with a 5% formalin solution. For heat-inactivation, viable oocysts were heated at 60 °C for 1 h in a dry bath incubator. All oocysts were stored at 4 °C in an antibiotic solution containing 0.01% Tween 20 (polysorbate 20) to prevent aggregation, 111 U penicillin, 111 U streptomycin, and 100 μg mL^{-1} of gentamicin (to prevent cell growth). All experiments were conducted within three months of the shed date of the oocysts.

Prior to performing the infrared spectroscopy experiments, oocysts were collected by centrifugation from the original suspension purchased from SPL. According to the supplier's specifications, centrifugation was performed at 13,000 rpm (17,900 rcf) for 2 min using an Eppendorf 5417 C microcentrifuge with a fixed angle rotor. The antibiotic supernatant solution was removed by pipette and replaced with 1 mL of 10 mM NaCl or 3.3 mM $CaCl_2$ solution at pH 6.0 (instead of deionized water to prevent cell plasmolysis). This procedure was repeated two more times to ensure the complete removal of all antibiotics, surfactant (Tween 20), and formalin (in formalin inactivated oocysts suspension). Oocysts were then resuspended by vortex mixing at a final concentration of 2×10^7 mL^{-1} in the electrolyte solution required for each FTIR experiment.

2.2. Solution preparation

Solutions were prepared in acid-washed vials using Barnstead Nanopure (BNP) water (Barnstead Thermolyne Nanopure Diamond UV water system, Dubuque, IA). All chemicals were ACS grade and were used without further purification. Monovalent electrolyte (NaCl) solutions were prepared at 1, 10, and 100 mM concentrations. Bivalent electrolyte ($CaCl_2$) solutions were prepared to give ionic strengths equivalent to those used for NaCl, i.e., corresponding millimolar concentrations of 0.33, 3.33, and 33.33, respectively. Solution pH was then adjusted to 3.0, 6.0, or 9.0 with HCl or NaOH (or $Ca(OH)_2$ in the case of $CaCl_2$ background electrolyte) solutions at the same ionic strength as the background solution. This $3 \times 3 \times 2$ experimental matrix (ionic strength × pH × cation type) resulted in testing 18 solution chemistries for each of three oocyst treatment conditions (viable, formalin-treated, and heat-treated), yielding a total of 54 different spectroscopic experiments.

2.3. Cryptosporidium oocysts characterization

The oocyst number concentration in experimental suspensions was measured using epifluorescence microscopy (Nikon, Optiphot

II). Oocysts were stained by contacting them with DNA-specific fluorescent dye 4,6-diamidino 2-phynulindole (DAPI, 0.1 mg L^{-1} solution) for 30 min prior to counting them manually with epi-fluorescence microscopy. The excitation and emission wavelengths used for DAPI-stained oocysts were 350 and 470 nm, respectively [9,33]. Average oocyst size was determined by immunofluorescent flow cytometry analysis of DAPI-stained samples (Biorad, HS Bryte) [33]. The average spherical diameter of oocysts was calculated to be 3.88 μm.

2.4. ATR-FTIR spectroscopy analysis

All ATR-FTIR experiments were conducted using a Magna-IR 560 Nicolet spectrometer (Madison, WI) equipped with a CsI beam splitter, a deuterated triglycine sulfate (DTGS) detector and OMNIC processing software. For each solution chemistry condition, an aliquot of the oocyst suspension (~500 μL) was introduced to the ATR cell by pipette. Spectra were obtained using a trough-style sample holder with a zinc selenide (ZnSe) internal reflection element (Spectra-Tech ARK ATR cell) (70 mm × 10 mm × 3 mm) subjected to a nominal incident angle of 45°, yielding 12 internal reflections at the sample surface [34]. The surface of the ZnSe IRE exhibits an isoelectric point <4 and relatively hydrophobic properties [28,35]. To examine the time dependence of surface interactions, spectra were collected as a function of time (mean times of 4, 19, 34, 64, and 124 min after sample introduction) at 25 °C. A volatile liquid cover was used to prevent solution evaporation. In addition, spectra were also collected after 24 h when the oocyst suspension had dried on the ATR crystal surface following removal of the volatile liquid cover.

Before running each sample, the ATR crystal surface was gently polished using nanoparticulate Al_2O_3 (<50 nm, Sigma–Aldrich) on a wet microcloth/cotton fibers (CleanTex), followed by rinsing with methanol and BNP water [36]. The crystal was considered clean if the stretching bands of CH_2 at ~2915 cm^{-1} and ~2850 cm^{-1} disappeared completely from the spectrum in single beam mode.

Spectra were collected as a function of pH, ionic strength, ionic composition, and surface treatment. For each spectrum, 400 scans were collected over the spectral range of 4000–800 cm^{-1} at a resolution of 4 cm^{-1} (collection time: 495 s). A final sample spectrum was obtained by subtracting that of the corresponding oocyst-free electrolyte solution from the spectrum of the suspension. The accurate subtraction scale factor is considered to be reached when the region from 1900 to 1740 cm^{-1} of the final spectrum is flat [37]. In every instance, the dry, clean 45° ZnSe crystal was used as the background. The spectrometer was continuously purged with CO_2 free air to eliminate CO_2 absorbance. Since baseline slope was not linear across the entire wavenumber range, multi-point baseline corrections with linear fits were performed for each spectrum using the OMNIC software. Peak fitting for quantitative comparisons was performed using GRAMS/AI software (Thermo Electron Co.). The areas of Lorentzian fitted peaks were used to quantify cell adhesion to the ZnSe IRE.

3. Results

3.1. ATR-FTIR spectra of oocysts

The ATR infrared spectra of oocysts show features similar to those of bacterial cells that have been published previously by several groups [25–31,38–40]. A representative ATR-FTIR spectrum of viable oocysts in 10 mM NaCl solution at pH 6 is shown in Fig. 1a (3000–2800 cm^{-1}) and Fig. 1b (1800–900 cm^{-1}). No residual purification reagents (sucrose and Percoll), antibiotics, or formaldehyde peaks were observed in the spectra, indicating their effective removal by the washing procedure. Band assignments are summarized in Table 1.

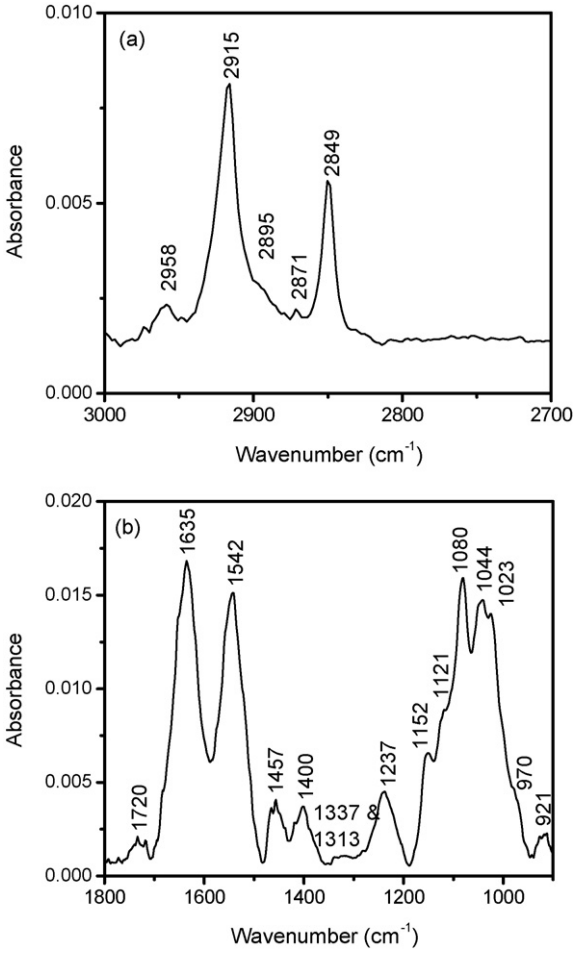

Fig. 1. ATR-FTIR spectrum of viable oocyst suspension on ZnSe IRE in 10 mM NaCl solution at pH 6 (a) 3000–2800 cm^{-1}; (b) 1800–900 cm^{-1}.

In the 3000–2800 cm^{-1} region, spectra are dominated by C—H stretching bands of fatty acid chains (Fig. 1a). The two strong bands at 2915 and 2849 cm^{-1} correspond to asymmetric and symmetric stretching of CH_2, respectively. The two relatively weak bands at

Table 1
Infrared absorption band assignments for *C. parvum* oocysts.

Wavenumber (cm^{-1})	IR band assignments
2958	ν_{as} (CH_3)
2915	ν_{as} (CH_2)
2871	ν_s (CH_3)
2849	ν_s (CH_2)
2895	ν_{as} (CH)
~1720	ν_{as} (COOH)
1635	Amide I: C = O, C—N, N—H
1542	Amide II: N—H, C—N
1457	δ (CH_2) scissoring
~1400	ν_s (COO^-)
1337–1313	Amide III: N—H, C—N, C—H, N—H
1237	ν_{as} (PO_2^-)
1152	Sugar ring vibration
1121	ν (C—O—P, P—O—P), ring vibrations
1080	ν_s (C—O—C, C—C), ν (PO_3^{2-})
1044	ν_s (C—O—C, C—C)
1023	Ring vibrations
970	ν_s (PO_2^-)
921	ν_{as} (O—P—O)

2958 and 2871 cm^{-1} originate from the asymmetric and symmetric stretching of CH_3. The shoulder at 2895 cm^{-1} corresponds to the stretching of CH. Relative intensities indicate CH_2 as a major component of the fatty acid chain with smaller fractions of CH_3 and CH. The band at 1457 cm^{-1} (Fig. 1b) originates from CH_2 bending vibrations.

From 1800 to 900 cm^{-1}, the spectra exhibit several distinct bands corresponding to carboxylate, amide, phosphate, and polysaccharide functionalities (Fig. 1b). The small band at 1720 cm^{-1} is probably a combination of two bands corresponding to the stretching of protonated carboxyl groups (COOH) and C=O of ester groups, whereas the peak at 1400 cm^{-1} corresponds to symmetric stretching of carboxylate (COO^-), and the asymmetric stretching of carboxylate (at *ca.* 1590 cm^{-1}) is masked by the intense amide II band. The region from 1700 to 1500 cm^{-1} is dominated by two distinct peaks at 1635 and 1542 cm^{-1}, corresponding to the amide I and amide II bands of proteins, respectively. Amide I results principally from stretching of carbonyl groups on proteins, while amide II results primarily from N—H bending. The broad, weak band between 1337 and 1313 cm^{-1} known as amide III results primarily from stretching of N—H and C—N. The distinct band at 1237 cm^{-1} is from symmetric stretching of phosphodiesters. Carbohydrates exhibit several bands in the region of 1150–950 cm^{-1}. Most of these bands can be assigned to sugar ring (C—O—C) and phosphate vibrations (C—O—P).

3.2. Oocyst surface interaction with the ZnSe IRE

3.2.1. Time dependence of the interaction

Addition of 500 μL of oocyst aqueous sample to the ATR-FTIR trough (70 mm × 10 mm) results in a suspension of cells with a water column depth of 0.714 mm. According to Stoke's law and assuming an oocyst particle density of 1.4 g cm^{-3}, all oocysts should sediment onto the IRE surface within 3 min. Nonetheless, infrared band intensities increased significantly throughout the first 34 min after suspension introduction (Fig. 2), which indicates that macromolecular re-orientation at the interface, an essential molecular-scale component of the oocyst adhesion process, proceeds long after physical settling has been completed. After 34 min reaction time, intensities of the bands in the spectral region 1600–1200 cm^{-1}, including the amide II band, appear to reach a maximum and no further increase is observed. However, the band intensities for carbohydrate (1150–950 cm^{-1}) and amide I (1635 cm^{-1}) continue to increase beyond 34 min (Fig. 2). Band intensities were normalized to that of amide II to assess the time-dependent change in biomolecular composition at the ZnSe surface [29]. After an initial decrease, normalized phosphate group absorbance (1237 cm^{-1}) remains almost constant for the duration of the experiment, whereas those of amide I (1635 cm^{-1}) and carbohydrate (1081 cm^{-1}) increase at longer times (Fig. 3). An increase in the intensity ratio of amide I:amide II is probably due to protein conformation/composition changes upon adhesion. Increased intensities of uncharged carbohydrates may be caused by oocysts more closely approaching the crystal surface with time (i.e., increased concentration of cells directly in contact with the crystal surface).

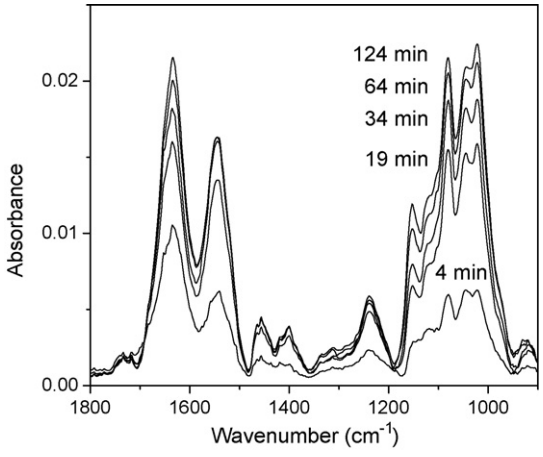

Fig. 2. ATR-FTIR spectra (1800–900 cm^{-1}) of oocysts in 3.3 mM $CaCl_2$ (pH 3) solutions on ZnSe IRE. Spectral intensity increases for 4, 19, 34, 64, and 124 min.

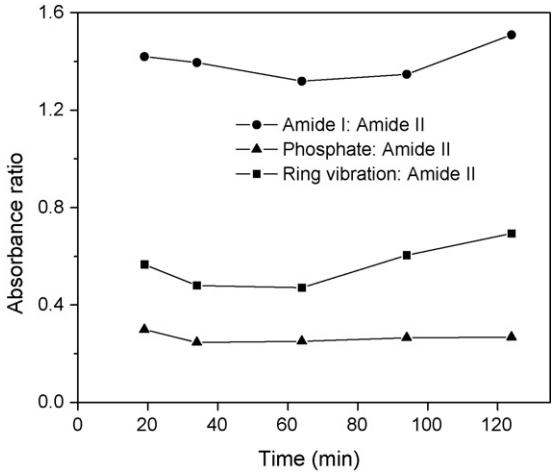

Fig. 3. IR absorbance ratios as a function of time for oocysts in 3.3 mM $CaCl_2$ (pH 3) solutions.

3.2.2. Solution chemistry effects

Since oocysts are typically 3–6 μm in size and the ATR-FTIR technique is sensitive only to bond vibrations in the sub-micrometer region (~0.5–1.5 μm, depending on incident radiation wavelength, for biological materials) of the IRE-aqueous sample interface [27]. ATR spectral data provide information on changes in surficial macromolecules involved in the oocyst adhesion process. Infrared absorbance, therefore, provides an index of the mass of microbial cells or adsorbed macromolecules in close proximity to the surface probed by the evanescent wave. Since subtraction of spectral background from H_2O (bending vibration at ~1630 cm^{-1}) may cause the variation in the absorbance of the amide I band, the absorbance of the amide II band has been often used as a measure of the concentration of proteins or bacterial cells that accumulate at the IRE interface in aqueous suspension [25,31,37].

In this study, the peak area of the amide II band (as fitted by GRAMS/AI software) was used as a measure of oocyst adhesion at the ZnSe surface. The results indicate that the adhesion behavior of oocysts in aqueous suspension is strongly affected by solution chemistry. Fig. 4 shows an example of the time-dependent variation in oocyst adhesion as a function of pH in 1 mM NaCl solution. No significant band changes or shifts were observed in the spectra, suggesting that surface functional groups are not detectably altered by changes in solution pH. Decreasing pH from 9.0 to 3.0 significantly increased oocyst adhesion, an observation that is consistent with column transport experiments [6,9]. This effect of pH was consistent across all solution chemistry and surface treatments (Fig. 5), although the difference between pH 6 and 9 was smaller for formalin than viable or heat-treated oocysts.

The effect of ionic strength (1.0, 10, or 100 mM) on oocyst adhesion was examined in both NaCl and $CaCl_2$ background solutions (Figs. 6–8). Increasing ionic strength from 1.0 to 100 mM sub-

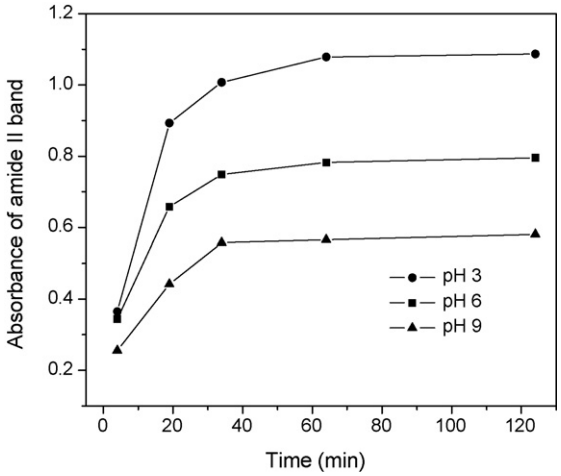

Fig. 4. Effect of pH on viable oocyst adhesion to ZnSe IRE in 1 mM NaCl solutions shown by the absorbance of the amide II band.

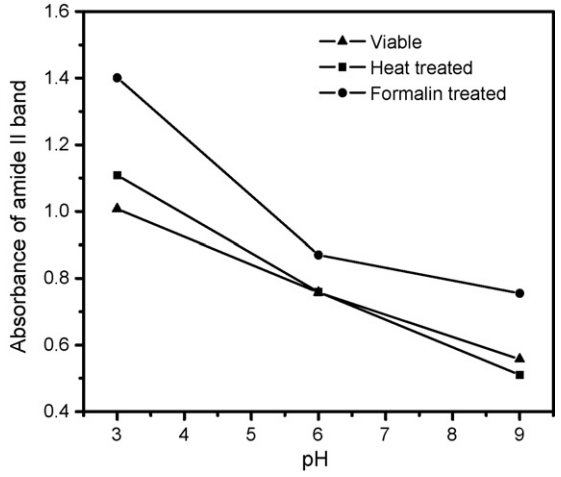

Fig. 5. Effect of pH on oocysts adhesion to ZnSe IRE in 1 mM NaCl solutions shown by the absorbance of the amide II band for 34 min reaction time.

stantially increased oocyst adhesion to the ZnSe surface. Infrared absorbance shows a log-linear correlation with ionic strength in both background electrolytes and all surface treatments (Figs. 7–8). Similarly, column transport experiments showed that retardation

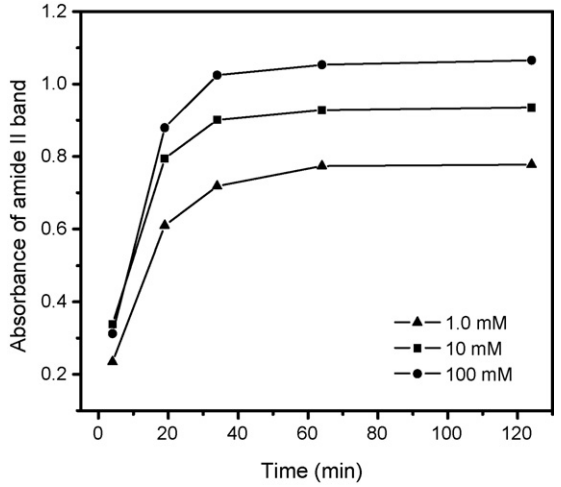

Fig. 6. Effect of ionic strength on viable oocysts adhesion to ZnSe IRE in $CaCl_2$ solutions at pH 6 shown by the absorbance of the amide II band.

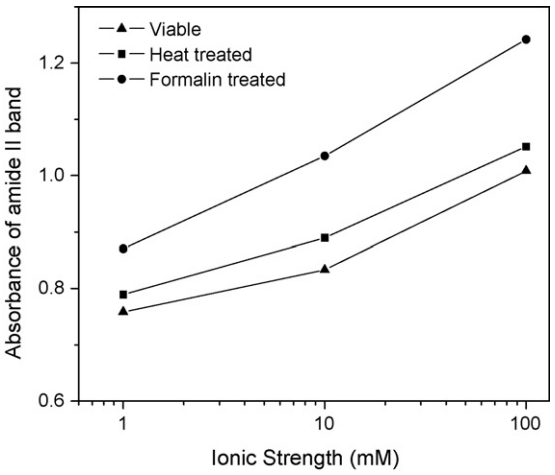

Fig. 7. Effect of ionic strength on oocysts adhesion to ZnSe IRE in NaCl solutions (pH 6) shown by the absorbance of amide II band for 34 min reaction time.

increases with ionic strength [6,12]. In contrast to the strong influence on adhesion of pH and ionic strength, the effect of cation composition (Na^+ versus Ca^{2+}) is relatively small and inconsistent (Fig. 8).

3.2.3. *Effects of inactivation treatments*

Both formalin and heat treatments increased oocyst adhesion to the IRE surface, with formalin having a larger effect (Figs. 5, 7, 9). Despite the fact that it is known to cross-link proteins, formalin treatment caused no ATR-FTIR detectable changes in the wavenumber and shape of the amide I or amide II bands (Fig. 10a). A small structural change was observed in the polysaccharide region of the spectra following formalin treatment. The peak assigned to sugar ring vibrations at 1023 cm^{-1} became sharper and more intense relative to neighboring peaks (Fig. 10b), suggesting a greater relative accumulation of polysaccharide functionalities at the IRE interface as a result of treatment with formalin.

Spectra of heat-treated oocysts were altered relative to viable forms in both the amide and the polysaccharide spectral regions. The amide I band shifted to lower wavenumber relative to its position in viable and formalin-treated oocyst suspensions (Fig. 10a). The polysaccharide region exhibits a similar change to that observed for the formalin treatment, with formation of an intense peak at 1023 cm^{-1} (Fig. 10b).

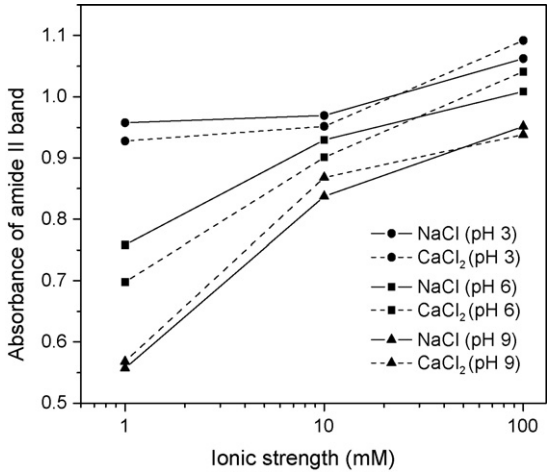

Fig. 8. Viable oocyst adhesion to ZnSe IRE in various background electrolytes as measured by the absorbance of the amide II band for 34 min reaction time.

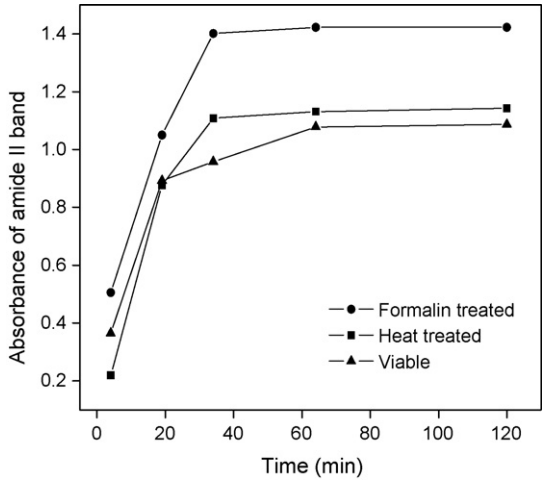

Fig. 9. Effect of surface modification on oocyst adhesion to ZnSe IRE in 1 mM NaCl (pH 3) solutions shown by the absorbance of the amide II band.

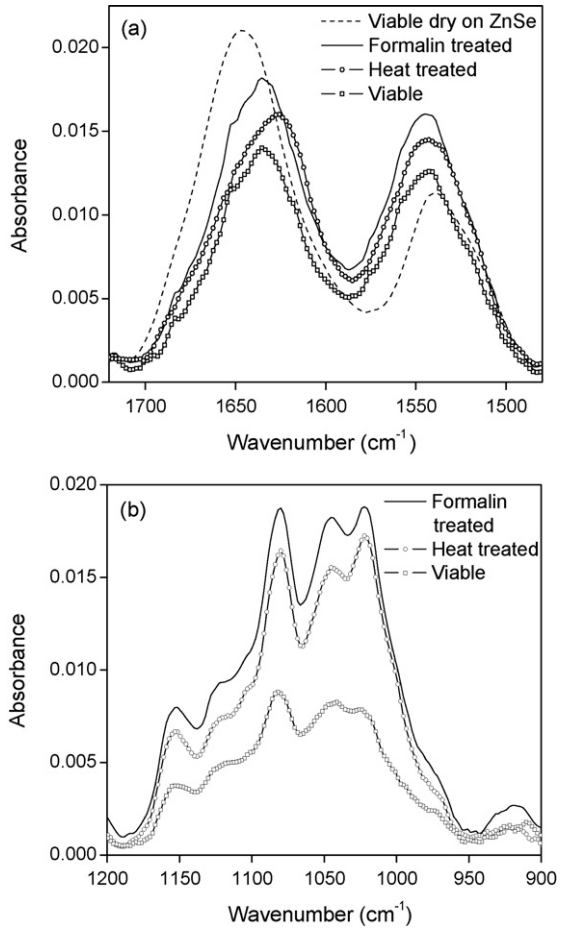

Fig. 10. (a) ATR-FTIR spectra (1720– 1480 cm^{-1}) of viable, formalin-, heat-treated oocyst suspension in 1 mM NaCl solutions (pH 3) for 34 min reaction time, and viable oocysts dry on ZnSe IRE surface (overnight without using volatile liquid cover, IR intensity reduced). (b) ATR-FTIR spectra (1200–900 cm^{-1}) of viable, formalin-, and heat-treated oocysts in 1 mM NaCl solutions (pH 3) on ZnSe IRE for 34 min reaction time.

4. Discussion

4.1. Effect of solution chemistry

Cell adhesion to solid surfaces in aqueous systems is governed by the electrostatic and van der Waals interactions described by DLVO theory, as well as by steric interactions between the cell surface polymers/macromolecules and solid surfaces [41]. The DLVO theory assumes smooth surfaces and generates a secondary energy minimum for cell adhesion [25]. Since microbial cells are composed of topographically complex mixtures of biomacromolecules with a diversity of functional groups distributed non-uniformly, classical DLVO theory cannot normally predict cell adhesion behavior [42]. The polymers at the cell surface may extend into solution because of electrostatic repulsion between them and the cell surface, producing a repulsive "electrosteric" force between cells and the solid surfaces. Numerous studies have recently demonstrated the importance of steric interactions in cell adhesion [1,10,18–20,43–45].

Cell adhesion may only occur when bonding interactions (e.g. protein binding, H-bonding, hydrophobic interactions, and polymer interactions) can overcome both the electrostatic and electrosteric repulsions between microbial cells and solid surfaces [29]. The adhesion of bacteria was reported to be inhibited by the DLVO-type electrostatic repulsive force at low ionic strength, but inhibition was dominated by steric interactions at high ionic strength [43]. Both types of interactions could be affected by solution chemistry (e.g. pH and ionic strength) [43,44]. Our results indicate that oocyst adhesion rate increased with increasing ionic strength and decreased with increasing pH, which is well explained by DLVO considerations alone.

In the case of pH variation, a decrease in electrostatic repulsive force was presumably accomplished by charge neutralization, i.e., direct protonation of weakly acidic surface sites. A change in pH affects ionizable functional groups on both oocysts and the ZnSe surface. Hence, to determine the electrostatic force between them, the surface charge of both should be considered. Oocysts are net negatively charged at pH >3, whereas the ZnSe crystal exhibits an isoelectric point at pH 4 [29], indicating that the crystal surface is net positively charged at pH 3, and net negatively charged at pH 6 and 9. The surfaces are expected to become more negatively charged with increasing pH above the isoelectric point. Adhesion of oocysts to the ZnSe therefore, is favored electrostatically at pH <4 where ZnSe and oocysts are oppositely charged, which explains why adhesion is much higher at pH 3 than at pH 6 and 9 (Fig. 5). In addition, as shown by Li and Tripp [46], cell adhesion to the IRE is enhanced not only by diminishing repulsive cell–IRE interactions, but also by diminishing repulsive cell–cell interactions (i.e., by protonating negatively charged cell surface functional groups). Since this phenomenon is expected to permit a higher packing density on the IRE surface, it may have contributed to the higher adhesion observed at pH 3 in the present study. Adhesion decreased significantly at pH 6 and 9 where both the ZnSe surface and oocyst are increasingly negatively charged.

In the case of increasing ionic strength, a decrease in the electrostatic repulsive force was accomplished by *charge screening* by the background electrolyte when oocysts and the ZnSe surface were of like charge (i.e., at pH >4). Increasing the cation concentration diminishes the repulsive force between the surfaces and favors oocyst adhesion. Supporting this interpretation is the fact that a charge screening effect is much less apparent at pH 3 than at pH 6 or 9 (Fig. 8). This suggests that the repulsive force between the ZnSe and oocysts is primarily electrostatic in nature, at least in the ionic strength range (1–100 mM) probed in this study [43].

For a given ionic strength, bivalent cations are known to more effectively reduce the electrostatic repulsion between two negatively charged surfaces than do monovalent cations – a manifestation of the "Schulze–Hardy rule" as it is applied to the stability of lyophobic colloids [47]. In addition, AFM studies have demonstrated that Ca^{2+} can compress the hairy layer at the oocyst surface and, therefore, reduce the electrosteric repulsion force [10]. However, no ATR-FTIR detectable change in oocyst adhesion rate was

observed between suspensions containing bivalent Ca^{2+} and monovalent Na^{+} in this experiment, indicating that the effect of ionic composition is small relative to effects of pH and ionic strength.

4.2. Influence of surface modifications

Formalin and heat inactivated oocysts are often used as surrogates for viable oocysts in laboratory studies because of the potential infection issues associated with the latter. Formalin is a protein cross-linking reagent that induces formation of covalent bonds between adjacent amine-containing functional groups [48]. Heat treatment is also effective to inactivate viable oocysts because exposure to high temperature causes protein denaturation. Whereas structural properties of the protein molecules are destroyed during the process, the covalent peptide bonds between amino acids remain intact [49]. In the present study, higher adhesion rate as measured by FTIR was consistently obtained after formalin and heat surface modifications. These results are consistent with the complementary studies of Kuznar and Elimelich [18] and Byrd and Walz [22] that used RSFS and AFM, respectively. These authors speculated that the increase in adhesion rate was due to macromolecular structural changes at the oocyst surface that resulted in a decrease in electrosteric repulsion.

Our results from ATR-FTIR provide a direct measure of surface structural change at the oocyst surface. For formalin treatment, no significant shift in frequency of the amide bands was observed in the spectra after treatment, but amide I:amide II band intensity ratios were altered. As the major component of formalin, formaldehyde (H_2CO) is thought to cross-link proteins by first adding one molecule of H_2CO to a primary amine on an amino acid to yield a hydroxymethyl ($—CH_2—OH$) intermediate. The hydroxymethyl group ($—CH_2—OH$) then condenses with a second primary amine to yield a methylene bridge ($—NH—CH_2—NH—$) [50]. According to the reaction mechanism, the oocyst surface should contain an overall decrease of N—H bonds and an increase of C—H bonds in the surface protein structures with no accompanying change in surface charge. The amide I: amide II intensity ratio increased after the formalin treatment (Fig. 11), which is consistent with a decrease in prevalence of N—H bonds due to the bridging reaction. A small structural change was also observed in the polysaccharide region of the spectra after formalin treatment. The intensity increase of the band at 1023 cm^{-1} corresponding to sugar ring vibrations may be caused by the ring structure change due to the treatment. In addition, while viable oocysts generally exhibit hydrophilic properties and the ZnSe surface is relatively hydrophobic [35], formalin treatment was reported to substantially increase the hydrophobicity of oocysts [18]. This enhancement of hydrophobicity may partially explain the increase in oocyst adhesion at the ZnSe surface.

For heat treatment, in addition to the change in the polysaccharide region of the spectra, a protein secondary structural change was observed, indicated by a shift in the amide I band due to the protein denaturation process. The results demonstrate that variation in oocyst adhesion may be related directly to heat-induced changes in the protein surface of the oocyst. These molecular-scale studies show, therefore, that use of formalin and heat inactivated oocysts as surrogates for viable cells in laboratory studies should be carefully considered since the treatments modify oocyst surface chemistry and affect the interaction mechanisms between oocysts and mineral substrates.

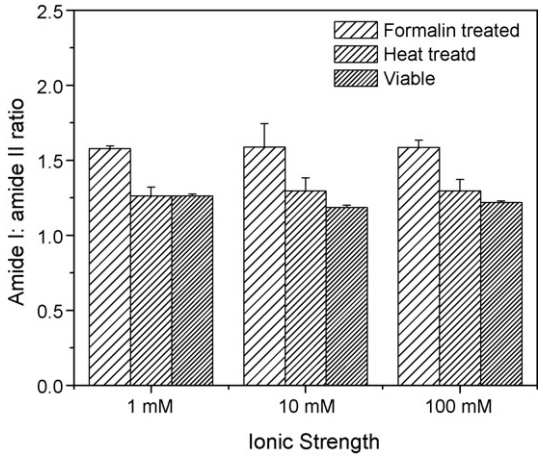

Fig. 11. Amide I:amide II absorbance ratios for viable, formalin-, and heat-treated oocysts as a function of ionic strength at pH 6.0 (34 min reaction time).

4.3. Protein secondary structural change

The secondary structure of proteins is sensitive to a change in microenvironment. The ATR-FTIR technique is capable of obtaining information on protein conformational changes in aqueous solutions [37]. Structural information can be obtained from the shape and wavenumber of the amide I band in the spectrum. The correlation between amide I frequencies and protein secondary structures has been well established [37,51,52]. Positioning of the amide I band in the range of 1658–1650 cm^{-1} is an indicator of α-helix conformers. The β-sheet vibrations usually occur between 1640 and 1620 cm^{-1}, with upper and lower frequencies representing the parallel and anti-parallel β-sheet, respectively. The major difference between them is the length of H-bonding, which is longer in the parallel (higher wavenumber) conformation. Absorbance at ~1646 cm^{-1} indicates the presence of random coil conformation.

Treatment-induced change in protein secondary structure was observed in the oocyst spectra. The amide I band was fitted with a Lorentzian function to determine the secondary structural components. The peak wavenumber, structural component assignment, and proportion of each component were summarized in Table 2. For viable oocysts suspensions, the amide I bands at 1630 and 1653 cm^{-1} indicate the presence of parallel β-sheet (70–80%) and α-helix (20–30%), respectively. When oocysts are dried on the ZnSe ATR crystal, the amide I band shifts to a symmetric peak at 1645 cm^{-1} (Fig. 11), indicating that a protein secondary structural change from β-sheet and α-helix to 100% random coil conformation due to the dehydration and denaturation processes. The fitting results for formalin-treated oocysts in suspension suggest no difference from viable form in secondary structural composition. Both exhibit about 70–80% parallel β-sheet and 20–30% α-helix conformation.

Table 2
Assignment of the amide I band to protein secondary structure as a function of treatment.

Treatments		Anti-parallel β-sheet 1623 cm^{-1}	Parallel β-sheet 1630 cm^{-1}	Random coil 1645 cm^{-1}	α-Helix 1658–1650 cm^{-1}
Suspension	Viable		70–80%		20–30%
	Formalin		70–80%		20–30%
	Heat	~60%			~40%
Dry on ATR				100%	

The amide I band clearly shifted to lower wavenumber after heat treatment. The shift from 1630 (viable) to 1623 cm^{-1} (heat-treated) is consistent with a change from parallel to anti-parallel β-sheet conformation, which implies a decrease in the protein H-bond lengths. This change signals an irreversible protein conformational changes that occurs during heat treatment and may reflect heat-induced dehydration. The shift from 1653 to 1650 cm^{-1} is difficult to interpret precisely. Both could be assigned as α-helix conformers. In addition, the proportion of α-helix increased more than 10% compared to that of viable oocysts.

5. Summary and conclusions

In-situ ATR-FTIR was used to investigate the surface chemistry of oocysts and the effects of solution chemistry and surface modification on oocyst adhesion to the ZnSe IRE surface. Results show that the dominant surface functional groups of oocysts are amide, phosphate, carboxylate, and polysaccharide. Oocyst adhesion to the ZnSe surface was strongly affected by solution chemistry. Increasing ionic strength or decreasing pH significantly increased the adhesion rate. In contrast, the effect of ionic composition is relatively small and the adhesion rate is essentially the same for both $CaCl_2$ and NaCl electrolytes for equivalent ionic strength. Formalin and heat treatments significantly improved oocyst adhesion. Results from ATR-FTIR provide direct evidence for oocyst surface chemistry changes after the surface treatments.

Acknowledgements

This research was supported by USDA, National Research Initiative, water and watersheds program (Grant #2006-35102-17192). We are grateful to Dr. Ronald Harvey and David Metge (USGS, Boulder, CO) for the use of the epifluorescence microscope and immunofluorescent flow cytometry instrumentation.

References

[1] Z.A. Kuznar, M. Elimelech, Environ. Sci. Technol. 38 (2004) 6839.
[2] L.J. Robertson, A.T. Campbell, H.V. Smith, Appl. Environ. Microbiol. 58 (1992) 3494.
[3] N. Tufenkji, D.R. Dixon, R. Considine, C.J. Drummond, Water Res. 40 (2006) 3315.
[4] W.R. Mackenzie, N.J. Hoxie, M.E. proctor, M.S. Gradus, K.A. Blair, D.E. Peterson, J.J. Kazmierczak, D.G. Addiss, K.R. Fox, J.B. Rose, J.P. Davis, N. Engl. J. Med. 331 (1994) 161.
[5] T. Harter, S. Wagner, E.R. Atwill, Environ. Sci. Technol. 34 (2000) 62.
[6] B.M. Hsu, C.P. Huang, J.R. Pan, Water Res. 35 (2001) 3777.
[7] N. Tufenkji, G.F. Miller, J.N. Ryan, R.W. Harvey, M. Elimelech, Environ. Sci. Technol. 38 (2004) 5932.
[8] N. Tufenkji, M. Elimelech, Environ. Sci. Technol. 39 (2005) 3620.
[9] R.A. Abudalo, Y.G. Bogatsu, J.N. Ryan, R.W. Harvey, D.W. Metge, M. Elimelech, Environ. Sci. Technol. 39 (2005) 6412.
[10] R.F. Considine, D.R. Dixon, C.J. Drummond, Water Res. 36 (2002) 3421.
[11] X. Dai, R.M. Hozalski, Water Res. 36 (2002) 3523.
[12] X. Dai, R.M. Hozalski, Environ. Sci. Technol. 37 (2003) 1037.
[13] M. Hermansson, Colloids Surf. B 14 (1999) 105.
[14] C.F. Brush, M.F. Walter, L.J. Anguish, W.C. Ghiorse, Appl. Environ. Microbiol. 64 (1998) 4439.
[15] C. Drozd, J. Schwartzbrod, Appl. Environ. Microbiol. 62 (1996) 1227.
[16] M.E. Karaman, R.M. Pashley, H. Bustamante, S.R. Shanker, Colloids Surf. A 146 (1999) 217.
[17] B. Hsu, C. Huang, Colloids Surf. A 201 (2002) 201.
[18] Z.A. Kuznar, M. Elimelech, Langmuir 21 (2005) 710.
[19] Z.A. Kuznar, M. Elimelech, Environ. Sci. Technol. 40 (2006) 1837.
[20] R.F. Considine, D.R. Dixon, C.J. Drummond, Langmuir 17 (2001) 6325.
[21] T.L. Byrd, J.Y. Walz, Environ. Sci. Technol. 39 (2005) 9574.
[22] T.L. Byrd, J.Y. Walz, Langmuir 23 (2007) 7475.
[23] J.R. Harris, F. Petry, J. Parasitol. 85 (1999) 839.
[24] F. Petry, Microsc. Microanal. 10 (2004) 586.
[25] M.J. McWhirter, P.J. Bremer, A.J. McQuillan, Langmuir 18 (2002) 1904.
[26] M.J. McWhirter, A.J. McQuillan, P.J. Bremer, Colloids Surf. B 26 (2002) 365.
[27] W. Jiang, A. Saxena, B. Song, B.B. Ward, T.J. Beveridge, S.C.B. Myneni, Langmuir 20 (2004) 11433.
[28] S.Y. Kang, P.J. Bremer, K.W. Kim, A.J. McQuillan, Langmuir 22 (2006) 286.
[29] S.J. Parikh, J. Chorover, Langmuir 22 (2006) 8492.
[30] A. Omoike, J. Chorover, Geochim. Cosmochim. Acta 70 (2006) 827.
[31] H.T.M. Heinrich, P.J. Bremer, C.J. Daughney, A.J. McQuillan, Langmuir 23 (2007) 2731.
[32] M.A. Butkus, J.T. Bays, M.P. Labare, Appl. Environ. Microbiol. 69 (2003) 3819.
[33] D.W. Metge, R.W. Harvey, R. Anders, D.O. Rosenberry, D. Seymour, J. Jasperse, Geomicrobiol. J. 24 (2007) 231.
[34] A. Omoike, J. Chorover, K.D. Kwon, J.D. Kubicki, Langmuir 20 (2004) 11108.
[35] S.J. Parikh, J. Chorover, Colloids Surf. B 62 (2008) 188.
[36] S.A. Dickie, A.J. McQuillan, Langmuir 20 (2004) 11630.
[37] K.K. Chittur, Biomaterials 19 (1998) 357.
[38] D. Naumann, D. Helm, H. Labischinski, P. Giesbrecht, The characterization of microorganisms by Fourier-transform infrared spectroscopy (FT-IR), in: W.H. Nelson (Ed.), Modern Techniques for Rapid Microbiological Analysis, VCH, New York, 1991, pp. 43–96.
[39] D. Naumann, C.P. Schultz, D. Helm, What can infrared spectroscopy tell us about the structure and composition of intact bacterial cells? in: H.H. Mantsch, D. Chapman (Eds.), Infrared Spectroscopy of Biomolecules, Wiley-Liss, New York, 1996, pp. 279–310.
[40] K. Brandenburg, U. Seydel, Fourier transform infrared spectroscopy of cell surface polysaccharides, in: H.H. Mantsch, D. Chapman (Eds.), Infrared Spectroscopy of Biomolecules, Wiley-Liss, New York, 1996, pp. 203–238.
[41] B.A. Jucker, H. Harms, S.J. Hug, A.J.B. Zehnder, Colloids Surf. B 9 (1997) 331.
[42] M.B. Salerno, B.E. Logan, D. Velegol, Langmuir 20 (2004) 10625.
[43] H.H.M. Rijnaarts, W. Norde, J. Lyklema, A.J.B. Zehnder, Colloids Surf. B 24 (1999) 179.
[44] T.A. Camesano, B.E. Logan, Environ. Sci. Technol. 34 (2000) 3354.
[45] S.L. Walker, J.A. Redman, M. Elimelech, Langmuir 20 (2004) 7736.
[46] H. Li, C.P. Tripp, Appl. Spectrosc. 62 (2008) 963.
[47] R.J. Hunter, Foundations of Colloid Science, Oxford University Press, New York, 2001.
[48] I.F.J. Eltoum, R.B. Myers, W.E. Grizzle, J. Histotechnol. 24 (2001) 173.
[49] M.T. Madigan, J.M. Martinko, J. Parker, Brock Biology of Microorganisms, 9th ed., Prentice Hall, Upper Saddle River, NJ, 2000.
[50] J.R. Kuykendall, M.S. Bogdanffy, Mutat. Res. 283 (1992) 131.
[51] J. Buijs, W. Norde, J.W.T. Lichtenbelt, Langmuir 12 (1996) 1605.
[52] F. Secundo, N. Guerrieri, J. Agric. Food. Chem. 53 (2005) 1757.